Applied Catalysis B: Environmental 101 (2011) 676–681

Contents lists available at ScienceDirect

Applied Catalysis B: Environmental

journal homepage: www.elsevier.com/locate/apcatb

Photocatalytic activity of TiO_2 thin films deposited by cathodic arc

A. Kleiman[a,b], A. Márquez[a,b,*], M.L. Vera[a,c], J.M. Meichtry[a,d], M.I. Litter[a,d,e]

[a] Consejo Nacional de Investigaciones Científicas y Técnicas, Buenos Aires, Argentina
[b] Instituto de Física del Plasma, CONICET, FCEN, Universidad de Buenos Aires, Ciudad Universitaria Pab. I, 1428 Buenos Aires, Argentina
[c] Facultad de Ciencias Exactas, Químicas y Naturales, Universidad Nacional de Misiones, Félix de Azara 1552, 3300 Posadas, Misiones, Argentina
[d] Gerencia Química, Comisión Nacional de Energía Atómica, Av. Gral. Paz 1499, 1650 San Martín, Prov. de Buenos Aires, Argentina
[e] Universidad Nacional de Gral, San Martín, Peatonal Belgrano 3563, 1650 San Martín, Prov. de Buenos Aires, Argentina

ARTICLE INFO

Article history:
Received 3 September 2010
Received in revised form 29 October 2010
Accepted 4 November 2010
Available online 11 November 2010

Keywords:
TiO_2
Thin films
Cathodic arc deposition
Heterogeneous photocatalysis
Cr(VI) photocatalytic reduction

ABSTRACT

In this work, the photocatalytic activity and the kinetic behavior of anatase TiO_2 films deposited by cathodic arc (*CA* films) on glass substrates are reported and compared with those of TiO_2 Degussa P-25 films obtained by dip-coating immersion (*DC* films). The mass density of films, determined by X-ray reflectometry was 20% lower for *DC* films compared with *CA* films, indicating a higher porosity of *DC* samples. The activity was evaluated from the efficiency to reduce Cr(VI) in the presence of EDTA. Although the response of *CA* films resulted lower compared with that of P-25 films of the same TiO_2 content (*e.g.* 90% *vs.* 50% Cr(VI) reduction after 180 min irradiation for samples with 0.03 mg cm^{-2} of TiO_2), a fact associated to the lower porosity, adhesion properties of the new materials were much better. *CA* film photoactivity improved by increasing the coating thickness; after 180 min, a sample with 0.03 mg cm^{-2} of TiO_2 presented 50% of Cr(VI) reduction *vs.* 80% for a sample with 0.28 mg cm^{-2}. These photocatalysts, whose preparation is simple and affordable, are very promising to be used as immobilized materials in photoreactors for the treatment of pollutants in gaseous and aqueous systems.

1. Introduction

Titanium dioxide has been the aim of numerous investigations due to its outstanding chemical and physical properties. One of the most active research fields on titania is its use as photocatalyst for degradation of pollutants, either in gases or water [1,2]. Small titania particles in aqueous suspension present a high photocatalytic activity for many pollutants; however, their use for water treatment requires a vigorous agitation throughout the reaction time and a final costly separation step. On the other hand, unsupported particles are not adequate for treatments in the gas phase. Therefore, recent investigations focused on the study of TiO_2 thin films deposited on glass substrates to avoid these drawbacks. In this way, degradation of contaminants in the catalytic photoreaction occurs by the heterogeneous reaction that takes place on the immobilized catalyst surface [3].

Among the different TiO_2 structures, anatase is the most active photocatalytic phase. From the available commercial materials, Degussa P-25, composed of *ca.* 9:1 anatase/rutile, presents an outstanding photocatalytic efficiency, and has been established as reference material [4].

TiO_2 thin films have been produced by several techniques, such as sol–gel [5], dip-coating [6–8], pulsed laser deposition [9], chemical vapor deposition [10] and physical vapor deposition [11]. Among the physical vapor deposition methods, cathodic arc deposition (CAD) is an efficient technique to produce thin films due to its high deposition rate and the high adherence of the coatings. The structure of the films produced by CAD depends significantly on the substrate temperature during the coating process. On glass substrates maintained at temperatures lower than 300 °C, TiO_2 grew amorphous, while at temperatures ranging from 300 to 400 °C, the films were deposited structured in the anatase phase. In the former case, amorphous films crystallized in anatase after a post-annealing step at 400 °C. However, the surface of the films crystallized *in situ* was less rough and had smaller grains, presenting typical grain sizes in the range 15–30 nm, 60% smaller than those of post-annealed samples [12].

In this work, the photocatalytic efficiency of anatase TiO_2 films grown by CAD on glass substrates at different temperatures is reported. The performance of these coatings was compared with those of TiO_2 Degussa P-25 films obtained by dip-coating immersion. The photocatalytic activity was evaluated by the efficiency to reduce hexavalent chromium in the presence of ethylenediaminetetraacetic acid (EDTA), a system very well studied by some of

* Corresponding author at: Instituto de Física del Plasma, CONICET, FCEN, Universidad de Buenos Aires, Ciudad Universitaria Pab. I, 1428 Buenos Aires, Argentina. Tel.: +54 11 4576 3371; fax: +54 11 4787 2712.
E-mail address: amarquez@df.uba.ar (A. Márquez).

0926-3373/$ – see front matter © 2010 Elsevier B.V. All rights reserved.
doi:10.1016/j.apcatb.2010.11.009

us [13–15]. Chromium (VI) is toxic and carcinogenic; for this reason, the World Health Organization recommends values for total chromium in drinking water not higher than 0.5 mg L^{-1} [16].

2. Experimental details

2.1. Film growth methods

The tested TiO_2 films were deposited by CAD using a DC vacuum arc and by dip-coating immersion into a P-25 suspension. The substrates for the samples were glasses with a coated area of 2 cm × 3 cm.

The vacuum arc device was described in detail in a previous work [17]. The arc was run with 120 A current between a Ti cathode and a grounded vacuum chamber serving as anode. The system was operated in an oxygen atmosphere with a continuous gas flux of 30 sccm and a working pressure in the range of 1–3 Pa. The substrates were located at 30 cm from the cathode surface on a grounded heater, which allowed fixing the substrate temperature with an accuracy of 10%. TiO_2 samples were obtained at both room temperature and at 400 °C. The coatings deposited at room temperature were treated with a post-annealing at 400 °C during 1 h in air at atmospheric pressure. The exposure time of the samples to the discharge was varied from 1 to 10 min in order to obtain different film thickness.

Dip-coating samples were prepared using a Degussa P-25 suspension (Degussa AG, Germany), 5% (w/v) at pH 2.5 ($HClO_4$, Merck, analytical reagent grade) in deionized water. The glass substrates were immersed once in the colloidal suspension and then pulled out at a constant withdrawal speed of 3.3 mm/s. Immediately after the impregnation, the coating on one of the faces of the glass was quickly eliminated. The sample was dried in a stove at 75 °C for 20 h, followed by a thermal treatment in a muffle at 400 °C during 1 h. The temperature of the muffle was incremented at a ramp rate of 7.5 °C/min up to 400 °C. Finally, the films were cooled naturally inside the muffle to room temperature.

Films grown by CAD at room temperature with the post-annealing treatment will be referred as *CART*, coatings deposited by CAD at 400 °C will be referred as *CAHT*, and films obtained by dip-coating, as *DC*.

2.2. Film characterization

The deposited TiO_2 mass was determined by weighing the samples before and after deposition using a Mettler balance, model AE 163, with a detection limit of 1×10^{-5} g. The crystalline structure of the films was identified by X-ray diffraction (XRD) using a Philips PW 3710 diffractometer with a CuK_α source. The analysis was performed on grazing angle geometry using a Philips thin film attachment, with an angle of incidence of 1°. The mass density of the films was determined by X-ray reflectometry (XRR) measurements carried out in the D12A-XRD1 beamline of the Brazilian Synchrotron Light Laboratory (LNLS) with photon energy of 8 keV. The bandgap of the films was estimated from the measurement of the transmittance employing a spectrophotometer (Shimadzu UV3101PC) over the wavelength (λ) range from 300 to 800 nm with an incident angle of 8°. Scotch and scratch tests were performed at the samples to evaluate the film adhesion. The scotch test was made with a commercial scotch tape. Since the films were transparent, the visual inspection was not reliable; therefore, the mass removal was studied by comparing the XRD spectra taken before and after the test. The scratch test was carried out with a Scratch Tester (CSEM REVESTEST) with a 0.2 mm radius Rockwell C diamond ended needle. The test was performed applying a progressive load with a maximum value of 10 N. The scratch length was 5 mm and the loading rate was 2 N/mm. After scratching, the samples were observed with an optical microscope.

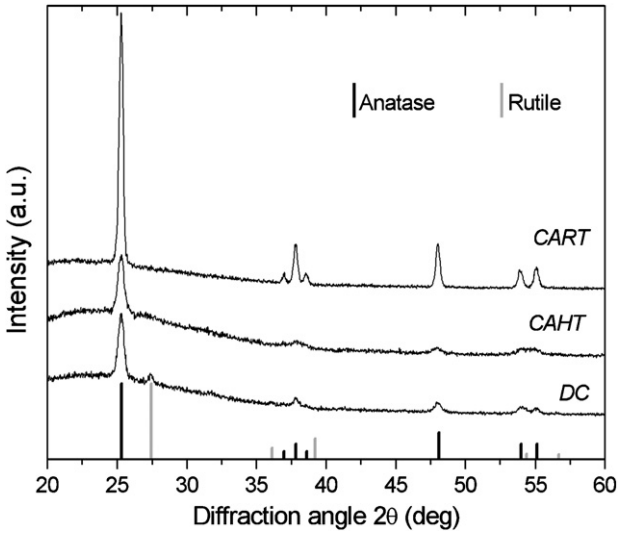

Fig. 1. X-ray diffraction patterns of the three types of films. Black and grey bars indicate the positions of the Bragg peaks corresponding to anatase and rutile, respectively.

2.3. Photocatalytic tests

A 0.4 mM $K_2Cr_2O_7$ (Merck) aqueous solution containing 1 mM EDTA (Riedel de Haën AG) was adjusted at pH 2 with 1 M $HClO_4$. This concentration was in the range of those used by some of us in previous papers [13–15]. The photocatalyst samples were immersed into 30 mL of this solution contained in a borosilicate glass Petri dish whose cap acted as filter for irradiation wavelengths lower than 300 nm. A Phillips HPA 400S UV lamp (250 nm < λ, maximum emission at 365 nm) was employed as light source. The mean UV irradiance was 5800 μW cm^{-2} (320 nm < λ < 400 nm), measured with a Spectroline model DM-365 XA radiometer.

Each system was irradiated for 6 h under continuous magnetic stirring. Samples of 1 mL were periodically taken from the solution and diluted 1/10 with water; when a TiO_2 suspension was used, the samples were filtered through a 0.2 μm cellulose acetate Sartorius membrane before analysis. Changes in Cr(VI) concentration were monitored by measuring the absorbance at 352 nm with a UV spectrophotometer (UV–vis HP 8453 A) [18]. An aqueous suspension of pure P-25, with a TiO_2 mass equivalent to that deposited by dip-coating was used as reference. Experiments were done at least by duplicate. The uncertainties in Cr(VI) concentrations were determined from the standard deviation of replicated experiments, being always lower than 12%.

Deionized water (18 MΩ cm), obtained from an E-pure Barnstead apparatus, was used for preparation of all solutions and washings.

3. Results and discussion

3.1. Characterization of samples

Typical XRD spectra obtained from *CART*, *CAHT* and *DC* films are shown in Fig. 1. The 2θ-positions of the Bragg peaks corresponding to TiO_2 in anatase and rutile phases are indicated in the figure. The coatings deposited with the vacuum arc exhibited only the anatase phase. The films obtained by dip-coating presented peaks associated to anatase phase and a small rutile phase peak, in agreement with the structure of the P-25 precursor [13].

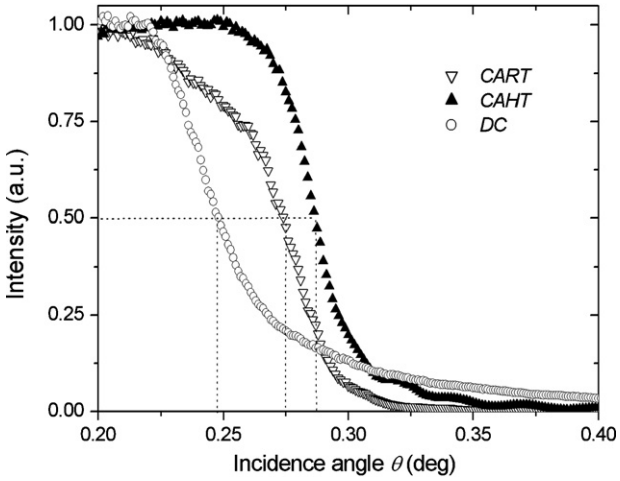

Fig. 2. Intensity of the reflected beam *vs.* incidence angle plots obtained for the three types of films by XRR at the LNLS (D12A-XRD1). Photon energy: 8 keV. Critical angles are indicated with dotted lines.

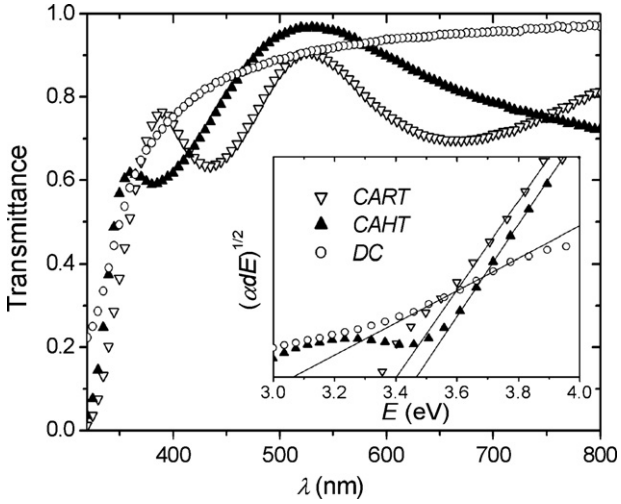

Fig. 3. Transmittance *vs.* wavelength (λ) plots obtained for the three types of films. The inset shows the extrapolation used to calculate the bandgap energies.

Typical XRR measurements for the three types of films are plotted in Fig. 2. At the smallest angles, the reflected intensity is maximal because the incident radiation causes total reflection. Beyond a critical angle, X-rays begin to penetrate the sample, and the collected intensity reduces rapidly. The critical angle positions (θ_c) were determined using Parratt's approximation, which assumes that the critical angle is that at which the reflected intensity is half the totally reflected intensity. In the small angle approximation, θ_c is related to the film mass density (ρ) as follows [19]:

$$\theta_c^2 = \frac{\lambda_x^2}{\pi} r_e N_A \rho \frac{Z + f'}{A} \quad (1)$$

where λ_x is the wavelength of X-rays, r_e is the classical electron radius, N_A is the Avogadro's number, Z the atomic number, A the atomic mass and $f' = 0.36$ (for TiO_2 and 8 keV) is the dispersion correction factor [20]. From the reflectivity profiles and using Eq. (1), ρ could be estimated. From θ_c measurements of different *CAHT* and *CART* samples, ρ values were found in the interval $(3.7 \pm 0.3)\ g\,cm^{-3}$, while for *DC* films ρ resulted $(2.9 \pm 0.1)\ g\,cm^{-3}$. The differences found between the densities could be associated to the porosity of the films, the coatings grown by CAD being more compact than those obtained by dip-coating.

Transmittance measurements as a function of the wavelength for the three types of films are depicted in Fig. 3. In the range $\lambda > 360$ nm, the transmittance was almost constant for *DC* samples, while for *CART* and *CAHT* samples the measurements presented some oscillations associated to an interference pattern that could be observed due to the high film homogeneity. The mean transmittance values (T_m) at $\lambda > 360$ were ~80%, ~85% and higher than 90% for *CART*, *CAHT* and *DC* samples, respectively. In the UV region, for $\lambda < 360$ nm, an important linear decrease in the transmittance value was observed; this behavior was attributed to the characteristic TiO_2 absorption in the UV region.

The bandgap energy (E_g) for the different samples was determined from the transmittance spectra. For $\lambda < 360$ nm, the absorption coefficient (α) can be related to the transmittance (T) according to the simplified expression [21] $\alpha d = -\ln(T)$, where d is the film thickness. Since TiO_2 allows indirect transitions, at energies somewhat above the E_g value, the relationship between α and E is expressed by [22]:

$$\alpha = \frac{A(E - E_g)^2}{E} \quad (2)$$

where E is the photon energy and A is a constant. E_g was determined from the plot of $(\alpha dE)^{1/2}$ *vs.* E at the absorption edge. The graphic of these variables is shown in the inset of Fig. 3. For *CART* and *CAHT* samples, E_g values were in the interval 3.40 ± 0.04 eV in agreement with values reported in the literature [23]. For *DC* films, the bandgap was significantly lower, 3.08 ± 0.03 eV, according to the expected bandgap of Degussa P-25 (3–3.2 eV) [24,25]. The uncertainties in the E_g values were determined from the extrapolation procedure.

The visual analysis of the surface after the scotch test indicated that the tape removed part of the film in the case of *DC* samples, while for *CART* and *CAHT* samples no detachment was observed. The comparison between the XRD spectra taken from the coated samples before and after the test corroborated that *DC* films were totally detached by the tape whereas the height of the XRD peaks did not change significantly (*i.e.* no mass removal was detected) for *CART* and *CAHT* films. Therefore, the scratch test was performed only to *CART* and *CAHT* samples. From this test, critical adhesion and cohesion loads were determined. Critical cohesion load was associated to the normal force applied by the scratch tester at the point where the film cracking was observed. Critical adhesion load was determined at the point where complete delamination of the coating was observed. Pictures of the scratch track for the different films are shown in Fig. 4. For *CART* films, from the beginning of the scratch channel, a discontinuous chip removing was observed (Fig. 4a), and a critical adhesion load of approximately 1 N was determined where the damage became continuous and complete delamination of the coating started (Fig. 4b). In the case of *CAHT* films, only cohesion fails were detected; the damage had the shape of shell-shaped spallation on the film (Fig. 4c). The critical cohesion load was assessed at 3 N.

3.2. Photocatalytic tests

In Fig. 5, typical results obtained from the photocatalytic tests for *CART* and *CAHT* films with a deposited mass by unit area (μ) of $0.038\ mg\,cm^{-2}$ are depicted. Normalized hexavalent chromium concentration (C/C_0) is plotted in the temporal profiles to circumvent slight differences in the initial run concentrations. As can be seen in the figure, films with the same μ independently of the growth temperature, showed similar activity, indicating that the photocatalytic response was not affected by the temperature employed during the growth process. The differences found in a previous work [12] about the surface roughness and the grain size between both types of films had no significant influence on their

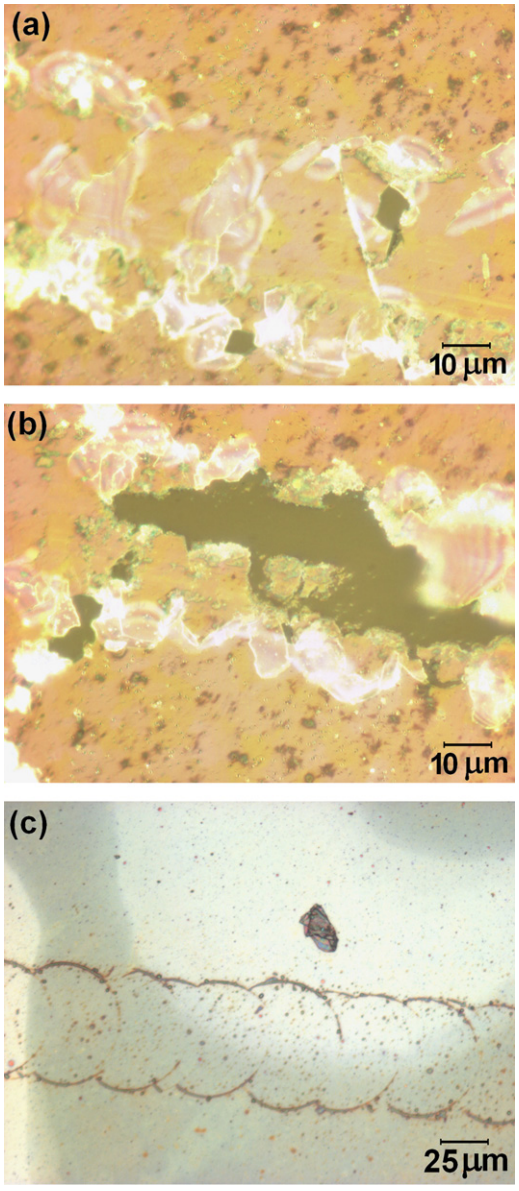

Fig. 4. Images obtained with an optical microscope after the scratch test. (a) *CART* film at the beginning of the scratch channel, (b) same *CART* film in the region of complete delamination and (c) *CAHT* film.

responses. Then, only two groups of samples were considered for further photocatalytic tests, *CA* films referring to films deposited by CAD (without distinction between *CART* and *CAHT*) and *DC* films.

In Fig. 6, the measured photocatalytic activity for *CA* samples with two different μ values (0.03 and 0.28 mg cm^{-2}), a *DC* film with μ = 0.03 mg cm^{-2} and a TiO_2 aqueous suspension with equivalent mass to *DC* film (6.5 mg L^{-1}) are compared. The activity of the Cr(VI)–EDTA system in the absence of photocatalyst (blank) is also shown.

Cr(VI) decay in the presence of TiO_2, either in suspension or supported, was faster in respect to the blank. Comparing films with similar masses, *DC* samples presented a higher activity than *CA* films, but lower than that of the TiO_2 aqueous suspension with equivalent mass. As expected, the suspension, even at so low concentration, is much more active than the immobilized photocatalyst (see *e.g.* Ref. [26]). The higher photoactivity of *DC* samples could be associated to the higher porosity of the films, as estimated from the density results (see Section 3.1). Higher photocatalytic activity related with higher porosity of TiO_2 samples has been

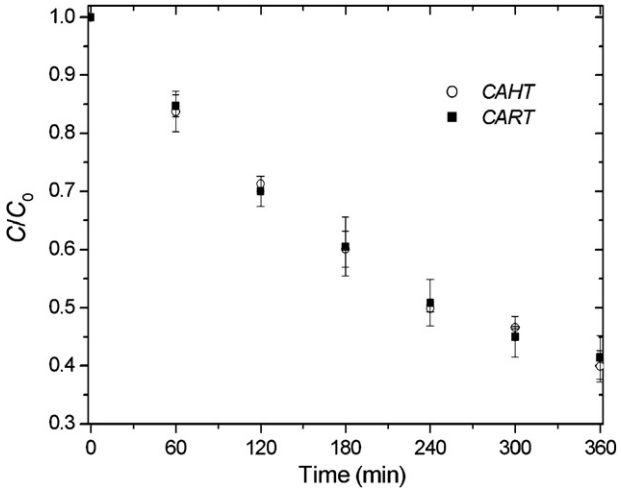

Fig. 5. Temporal evolution of normalized Cr(VI) concentration during photocatalytic tests for *CART* and *CAHT* films with a deposited mass by unit area (μ) of 0.038 mg cm^{-2}. Conditions: [Cr(VI)] = 0.8 mM, [EDTA] = 1 mM, pH 2, λ_{max} = 365 nm, irradiance = 5800 μW cm^{-2}.

found in several works (see for example, Ref. [27]). Rate of *CA* films increased with μ, reaching a total Cr(VI) reduction at 360 min for the case μ = 0.28 mg cm^{-2}.

The kinetic behavior of the different systems merits a further analysis. In the absence of organic compounds, at the experimental conditions of the present study, Cr(VI) is not photoreducible by near UV light. However, although the dark thermal reaction is almost negligible, Cr(VI) reduction is enhanced under UV irradiation in the presence of some alcohols and carboxylic acids due to inner- or outersphere charge transfer between the chromate anion and the organic compound [28,29]. Therefore, in the presence of EDTA, a homogeneous photoreduction of Cr(VI) takes place (blank), whose experimental points could be adjusted by a first order kinetic equation:

$$\frac{-d(C/C_0)}{dt} = \frac{kC}{C_0} \quad (3)$$

where k is the kinetic constant for the homogeneous process.

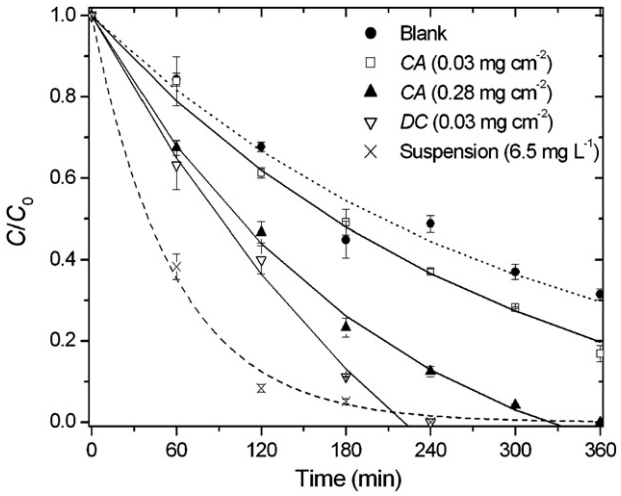

Fig. 6. Temporal evolution of normalized Cr(VI) concentration during photocatalytic tests for different types of films, for TiO_2 aqueous suspension with equivalent mass to *DC* film and for Cr(VI)–EDTA system in the absence of photocatalyst (blank). Conditions: [Cr(VI)] = 0.8 M, [EDTA] = 1 mM, pH 2, λ_{max} = 365 nm, irradiance = 5800 μW cm^{-2}. Dotted, dashed and solid lines show the best fits of the experimental data with Eqs. (3), (4) and (5), respectively.

Table 1
Rate constants for Cr(VI) decay corresponding to data presented in Fig. 6.

Experiment	k ($\times 10^{-3}$ min^{-1})[a]	k'_0 ($\times 10^{-3}$ min^{-1})[b]	R^2
Blank	3.4 ± 0.8	–	0.969
CA (0.03 mg cm^{-2})	3.4	0.5 ± 0.1	0.994
CA (0.28 mg cm^{-2})	4.9	1.3 ± 0.1	0.997
DC (0.03 mg cm^{-2})	3.4	3.1 ± 0.6	0.995

[a] k, determined with Eq. (3) for the blank.
[b] k'_0, determined with Eq. (5) only for the immobilized catalysts, taking k from the blank corresponding to the same run.

In respect to the photocatalytic experiments, Cr(VI) decay using a TiO_2 suspension followed a simple first order regime, and could be fitted with:

$$\frac{-d(C/C_0)}{dt} = \frac{k'C}{C_0} \quad (4)$$

where k' is the rate constant for the photocatalytic process. Other authors found a similar kinetic behavior [30–32].

In contrast, when the supported photocatalysts were used, a more complex kinetics was followed. The experimental points had to be adjusted by Eq. (5), composed of a first order term to account for the photolytic homogeneous reaction plus a zero order term describing the heterogeneous reaction on the immobilized catalyst surface:

$$\frac{-d(C/C_0)}{dt} = \frac{kC}{C_0} + k'_0 \quad (5)$$

where k'_0 is the rate constant of the photocatalytic reaction and k is the kinetic constant for the homogeneous process. The zero order regime for the photocatalytic process with immobilized TiO_2 can be rationalized by considering that, under the experimental conditions, the area covered with TiO_2 is small compared to the total area of particles in suspension. Thus, the area of the immobilized catalyst is saturated by adsorbed Cr(VI) at all the times during the photocatalytic run [33], making the reduction rate independent from Cr(VI) concentration in solution.

The fitting curves using Eqs. (3)–(5) are represented in Fig. 6, and they present a good agreement with the experimental points. The k' value obtained from the fitting of the suspension was 0.017 ± 0.002 min^{-1} ($R^2 = 0.996$). In Table 1, the values of the corresponding rate constants for the blank and the films are shown. The k values for the immobilized catalysts were determined from the blank corresponding to the same run. The different value of k for the *CA* sample is due to small differences in the temperature at which the runs were performed, as the homogeneous reaction is sensitive to temperature (Meichtry and Litter, ongoing results).

The dependence of the reaction efficiency on the film thickness (proportional to μ) can be extracted from Fig. 7, where k'_0 as a function of μ for *CA* films is plotted. The uncertainties were determined for k'_0 from the fitting and for μ from uncertainties in the mass and area measurements.

It can be observed that the rate of degradation increased as μ increased. When the diffusivity of the reagents and the optical thickness are high, the degradation rate of a photocatalytic reaction increases with the film thickness until a specific thickness value at which the degradation rate is not significantly enhanced anymore, tending to an asymptotic value [34]. The performance found within the studied μ range in Fig. 7 agrees with a system in which the asymptotic behavior of the degradation rate was still not achieved, i.e. limited neither by the optical thickness nor by the internal mass transfer resistance resulting from the diffusion of the reactant through the catalyst film.

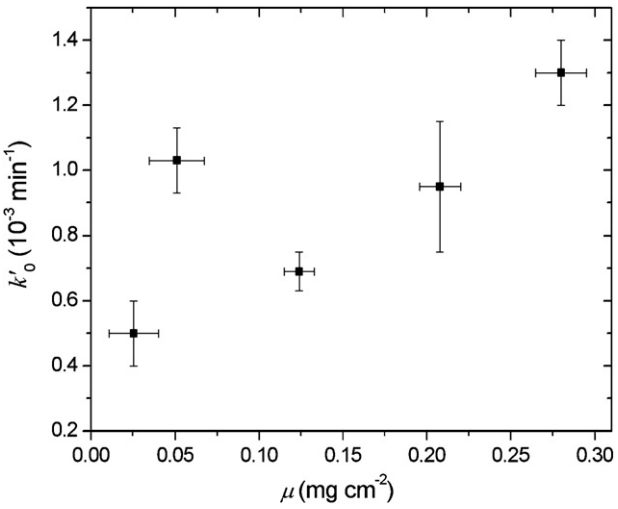

Fig. 7. Rate constant of the photocatalytic reaction (k'_0) as a function of the deposited mass by unit area (μ) for *CA* films.

4. Conclusions

The kinetic behavior observed for Cr(VI) TiO_2 photocatalytic reduction using immobilized photocatalysts differed from that using TiO_2 in suspension. While a first order regime was observed using suspensions, for films, the kinetics was driven by contributions of both the photolytic reaction and the heterogeneous reaction on the immobilized catalyst. A more comprehensive study on this issue is underway. *DC* films shown higher photoactivity for Cr(VI) reduction in the presence of EDTA than *CA* films; while a *CA* film presented a Cr(VI) reduction of 50% after 180 min irradiation, a *DC* film of the same TiO_2 content (0.03 mg cm^{-2}) presented a 90% reduction at the same time. This fact could be associated to the higher porosity presented by *DC* films, as the density of *DC* films was a 20% lower than that of *CA* films. On the other hand, the differences in morphology between *CART* and *CAHT* films had no effect on the photoactivity, as it would have been expected due to the noticeable differences in grain size structure. The reaction efficiency increased as the deposited mass per unit area increased, not reaching saturation along the studied thickness range, but attaining a 100% of Cr(VI) reduction after 6 h of irradiation in the case $\mu = 0.28$ mg cm^{-2}. Therefore, the efficiency of *CA* films could be enhanced by increasing the thickness until a limiting value. Adhesion tests demonstrated that *DC* films have a very poor adhesion, while *CAHT* presented the best adhesion properties. Thus, *CAHT* films with the thicker thickness presented the best performance for photocatalytic applications. These photocatalysts, whose preparation is simple and affordable, are very promising to be used as immobilized materials in photoreactors for the treatment of pollutants not only in the gas phase but also in aqueous systems.

Acknowledgements

This work was supported by grants of Universidad de Buenos Aires and Agencia Nacional de Promoción Científica y Tecnológica (PAE22257, PICT512 and PICT38251). XRR measurements were performed at LNLS (6060-D12A-XRD1-8693). The authors would like to thank Diego Lamas for XRD studies at CINSO (CITEFA-CONICET), Enrique San Román and Martín Mirenda for transmittance measurements at DQIAQF (FCEN-Universidad de Buenos Aires) and Elena Forlerer for performing the scratch test at CAC-CNEA.

References

[1] M. Kitano, M. Matsuoka, M. Ueshima, M. Anpo, Appl. Catal. A 325 (2007) 1–14.
[2] M.I. Litter, Appl. Catal. B 23 (1999) 89–114.
[3] M.F.J. Dijkstra, H. Buwalda, A.W.F. de Jong, A. Michorius, J.G.M. Winkelman, A.A.C.M. Beenackers, Chem. Eng. Sci. 56 (2001) 547–555.
[4] D.C. Hurum, A.G. Agrios, K.A. Gray, T. Rajh, M.C. Thurnauer, J. Phys. Chem. B 107 (2003) 4545–4549.
[5] L. Sun, T. An, S. Wan, G. Li, N. Bao, X. Hu, J. Fu, G. Sheng, Sep. Purif. Technol. 68 (2009) 83–89.
[6] C.J. Brinker, A.J. Hurd, J. Phys. III (France) 4 (1994) 1231–1242.
[7] G. Piperata, J.M. Meichtry, M.I. Litter, Prog. Colloid Polym. Sci. 128 (2004) 303–308.
[8] J.M. Meichtry, H.J. Lin, L. de la Fuente, I.K. Levy, E.A. Gautier, M.A. Blesa, M.I. Litter, J. Solar Energy Eng. 129 (2007) 119–126.
[9] M.F. Brunella, M.V. Diamanti, M.P. Pedeferri, F.D. Fonzo, C.S. Casari, A.L. Bassi, Thin Solid Films 515 (2007) 6309–6313.
[10] Y. Hatanaka, H. Naito, S. Itou, M. Kando, Appl. Surf. Sci. 244 (2005) 554–557.
[11] O. Zywitzki, T. Modes, H. Sahm, P. Frach, K. Goedicke, D. Glöß, Surf. Coat. Technol. 180–181 (2004) 538–543.
[12] A. Kleiman, A. Márquez, D.G. Lamas, Surf. Coat. Technol. 201 (2007) 6358–6362.
[13] M.L. Vera, Preparación de fotocatalizadores de TiO_2 soportados para su uso en potabilización de aguas, Master Thesis, Instituto de Tecnología Prof. Jorge A. Sabato, Universidad Nacional de General San Martín, Buenos Aires, 2008.
[14] J.A. Navío, J.J. Testa, P. Djedjeian, J.R. Padrón, D. Rodríguez, M.I. Litter, Appl. Catal. A 178 (1999) 191–203.
[15] J.J. Testa, M.A. Grela, M.I. Litter, Langmuir 17 (2001) 3515–3517.
[16] Guidelines for Drinking-water Quality, 3rd ed., Incorporating 1st and 2nd Addenda. Vol. 1, Recommendations, World Health Organization, 2006.
[17] A. Márquez, G. Blanco, M.E. Fernandez de Rapp, D.G. Lamas, R. Tarulla, Surf. Coat. Technol. 187 (2004) 154–160.
[18] W.-Y. Lin, C. Wei, K. Rajeshwar, J. Electrochem. Soc. 140 (1993) 2477–2482.
[19] L.G. Parrat, Phys. Rev. 95 (1954) 359–369.
[20] B.L. Henke, E.M. Gullikson, J.C. Davis, At. Data Nucl. Data Tables 54 (1993) 181–342.
[21] H. Kuzmany, Solid-State Spectroscopy: An Introduction, Springer-Verlag, Berlin, 1998.
[22] J. Tauc, Mater. Res. Bull. 5 (1970) 721–729.
[23] H. Takikawa, T. Matsui, T. Sakakibara, A. Bendavid, P.J. Martin, Thin Solid Films 348 (1999) 145–151.
[24] R.I. Bickley, T. Gonzalez-Carreno, J.S. Lees, L. Palmisano, R.J.D. Tilley, J. Solid State Chem. 92 (1991) 178–190.
[25] S.T. Martin, H. Herrmann, M.R. Hoffmann, J. Chem. Soc. Faraday Trans. 90 (1994) 3323–3330.
[26] M.N. Chong, B. Jin, C.W.K. Chow, C. Saint, Water Res. 44 (2010) 2997–3027.
[27] C.A. Emilio, J.J. Testa, D. Hufschmidt, G. Colón, J.A. Navío, D.W. Bahnemann, M.I. Litter, J. Ind. Eng. Chem. 10 (2004) 129–138.
[28] P. Mytych, P. Ciesla, Z. Stasicka, Appl. Catal. B 59 (2005) 161–170.
[29] P. Ciesla, P. Kocot, P. Mytych, Z. Stasicka, J. Mol. Catal. A 224 (2004) 17–33.
[30] M.R. Prairie, L.R. Evans, B. Stange, S.L. Martínez, Environ. Sci. Technol. 27 (1993) 1776–1782.
[31] L. Wang, N. Wang, L. Zhu, H. Yu, H. Tang, J. Hazard. Mater. 152 (2008) 93–99.
[32] G. Cappelletti, C.L. Bianchi, S. Ardizzone, Appl. Catal. B 78 (2008) 193–201.
[33] F. Hongxiang, L. Gongxuan, L. Shuben, Adsorpt. Sci. Technol. 16 (1998) 117–126.
[34] G. Camera-Roda, F. Santarelli, Catal. Today 129 (2007) 161–168.